International Journal of Multiphase Flow 75 (2015) 163–173

Contents lists available at ScienceDirect

International Journal of Multiphase Flow

journal homepage: www.elsevier.com/locate/ijmulflow

Effect of bubble size on void fraction fluctuations in dispersed bubble flows

Sotiris P. Evgenidis, Thodoris D. Karapantsios *

Division of Chemical Technology, School of Chemistry, Aristotle University, University Box 116, 541 24 Thessaloniki, Greece

ARTICLE INFO

Article history:
Received 24 November 2014
Received in revised form 20 May 2015
Accepted 25 May 2015
Available online 3 June 2015

Keywords:
Dispersed bubble flow
Void fraction
Bubble size
Electrical impedance
Signal analysis

ABSTRACT

It is known that bubble size affects seriously the average void fraction in bubbly flows where buoyant velocities vary considerably with bubble size. On the contrary, there is no systematic literature report about bubble size effects on the intensity and frequency of void fraction fluctuations around the average void fraction. This work aims to provide such information. An electrical impedance technique is employed along with non-intrusive ring electrodes to register void fraction fluctuations down to 10^{-5}. Bubble size fluctuations are estimated from high resolution optical images. Experiments are conducted in co-current upward dispersed bubble flow inside a 21 mm tube with average bubble size between ~50 and ~700 μm. Water and blood simulant are used as test liquids with velocity from ~3 to ~30 cm s^{-1}. The above resemble conditions of Decompression Sickness (DCS) in the bloodstream of human vena cava. It is found that the intensity and frequency of void fraction fluctuations vary appreciably with bubble size at constant gas and liquid flow rates. Moreover, these variations are not random but scale with bubble size. As a first step to quantify this effect, an empirical expression is derived that relates average bubble size to the ratio standard deviation/average value of void fraction.

Introduction

Bubbly (multiple-bubble) flow is a very common type of gas–liquid two-phase flow characterized by the existence of discrete gas bubbles dispersed in a continuous liquid phase. Bubbly flow is encountered in a variety of industrial processes, e.g. chemical and petroleum processing, oil and gas extraction and transportation, nuclear power generation, etc (Das and Das, 2010; Shen et al., 2005). It is also encountered in the human bloodstream during Decompression Sickness incidents, e.g. in astronauts, scuba divers and metro workers (Papadopoulou et al., 2013).

Void fraction (volumetric gas fraction) is a very important physical parameter in all kinds of two-phase flow. Numerous experimental techniques have been developed to measure void fraction in integral or local fashion including quick shut valve methods, image processing methods, X-ray CT scan methods, neutron radiography methods, gamma-ray method, NMR and so on. The aforementioned methods are subjected to various technical restrictions and, additionally, they are hard to apply for capturing high frequency temporal fluctuations of void fraction (Uesawa et al., 2012). Electrical impedance measurements are free of such drawbacks. Electrical impedance depicts quantitatively the distribution of a two phase mixture close to a system of measuring electrodes as much as the electrical properties of the two phase components are sufficiently different from each other, e.g. water and air (Devia and Fossa, 2003).

There are many different possibilities to arrange a system of electrodes –intrusive or non-intrusive- for void fraction measurement purposes (Ceccio and George, 1996). In a few studies, the size of large isolated bubbles has been determined by means of intrusive dual impedance probes in two-phase flow applications (Tang and Fan, 1989; Liu, 1993; Chen et al., 1998). Non-intrusive, flush mounted onto the vessel wall ring electrodes were first employed by Asali et al. (1985), while Andreussi et al. (1988) and Tsochatzidis et al. (1992) developed the theoretical basis regarding the response of this electrode configuration, which has been further employed in several three-phase applications, e.g. Begovich and Watson (1978) and Karapantsios et al. (1993).

It must be stressed that most of the earlier efforts were devoted to accurate measurement of the average void fraction where void fraction fluctuations were seen only as a statistical measure of discrepancy. On this account, it has been realized that the separation distance between electrodes is critical in order to obtain meaningful average data. In many cases examined in literature, the selection of the separation distance between electrodes has been

* Corresponding author. Tel./fax: +30 2310997772.
E-mail address: karapant@chem.auth.gr (T.D. Karapantsios).

http://dx.doi.org/10.1016/j.ijmultiphaseflow.2015.05.013
0301-9322/

based on the volume-averaging approach of modeling porous media (e.g. Carbonell and Whitaker, 1984). According to this approach, the size of the probe averaging volume, i.e., the required minimum volume surrounding a probe has to be large enough to average void fraction fluctuations, e.g., due to the finite bubble size, yet small enough to preserve the local character of the measurements (Celmins, 1988). So in most cases void fraction fluctuations caused by a flowing bubble swarm were sacrificed to obtain an accurate average value of void fraction. Nevertheless, large void fraction fluctuations may jeopardize the control schemes in operating industrial equipment. Furthermore, void fraction fluctuations may serve as indicator of process performance, e.g. efficient mixing, degree of dispersion etc.

In common bubbly flows, one would expect average bubble size to affect average void fraction at constant gas and liquid flow rates. But this is different from how average bubble size may affect void fraction fluctuations. The latter has to do with the spatial and temporal characteristics of the sensing probe, i.e., with the disturbance of the electric field as bubbles flow through the measuring volume and pass over the electrodes (Devia and Fossa, 2003). Bubbles flowing close to the surface of electrodes have stronger effect than those far away in the measuring volume but this effect scales also with the size of bubbles with respect to the width of the electrodes. The overall electrical response is an instantaneous average along the total electrode's surface and across the entire measuring volume so the effect of single bubbles is diminished (Tsochatzidis et al., 1992).

To our knowledge, there is no report in literature that systematically quantifies the effect of bubble size of a flowing bubble swarm on void fraction fluctuations. In order to obtain such information without compromising the accuracy of the average void fraction measurement, techniques of superb sensitivity are required. Such information is also important when one wants to estimate average void fraction values from electrodes placed not far apart along the flow which usually leads to intense void fraction fluctuations. Closely spaced electrodes may be required due to spatial constraints or because of the evolving nature of the flow (not fully developed flow). On the other hand, it is extremely useful if one can obtain simultaneous information on the average void fraction and the average bubble size (from void fraction fluctuations). The latter is the motivation for this study.

Herein, we exploit electrical impedance measurements of high temporal and spatial resolution taken with non-intrusive ring electrodes in order to correlate void fraction fluctuations to bubble size in a co-current upward bubbly flow. The examined conditions resemble bubbly flow in human vena cava during Decompression Sickness (DCS). However, the methodology can be extended to any kind of bubbly flow. Since the measurement of void fraction values lower than 10^{-2}, that interest mostly the present study, fall within the noise level of conventional electrical techniques (Karapantsios and Papara, 2008), a novel electrical impedance technique has been developed (Evgenidis, 2011). Innovative hardware and signal analysis/processing have improved the sensitivity about two orders of magnitude compared to conventional techniques allowing capturing of void fraction fluctuations down to 10^{-5}.

In the following section, the experimental setup is outlined along with the employed measuring technique. A section follows on experimental results and discussion on the performance of the technique.

Materials and methods

Measurements are conducted in vertical co-current upward bubbly flow. Flow is provided by a fully controllable flow loop made of PMMA tubing capable of generating steady and pulsatile flow at various liquid/gas flow rates and bubble sizes. Only steady flow is employed in this study. The main part of the loop consists of a vertical tube 1.6 m long with $D = 21$ mm. This is the diameter of human vena cava where bubbles gather during a decompression incident (Vann et al., 2011). In Fig. 1, the small orthogonal blocks along the vertical tube stand for test sections of electrical, optical, acoustical and pressure diagnostics. These sections are separated by flanges and so can be interchanged. Diagnostics are meant for void fraction measurement and identification of bubbles characteristics. In this work, acoustical measurements were not performed.

The liquid phase is recirculated through the flow loop by means of a progressive cavity pump (MD 025-6L, Motovario S.p.A.) providing cavitation-free and pulseless flow even at low rates. The temperature of the flowing liquid remains constant at the desired value within ±0.1 °C, using a heater/circulator (HAAKE C10-P5/U, Thermo Electron Corporation, HC-1, Fig. 1) which is immersed in the liquid tank (T-1, Fig. 1). The gas phase is injected through a cylindrical glass micro-porous filter (ROBU®; 10 mm diameter, 20 mm length, 1.6 μm nominal pore size) located at the center of the bottom of the vertical tube, where the two phases come in contact. The liquid enters the vertical tube through the annulus formed between the filter and the tube walls. Bubbles enter the flow after being sheared-off from the side walls of the filter by the annular liquid flow. The top side of the filter is plugged with glue to avoid entrance of larger bubbles into the flow.

Void fraction measurements are conducted with a patented ultra-sensitive electrical impedance technique (Karapantsios et al., 2014). A sinusoidal voltage signal (V_i) with a frequency of 25 kHz and amplitude of 2 Vp–p is applied to a ring electrode in order to excite electrically the bubbly flow inside the tube, generating an input current passing through the medium. For gas/liquid two phase systems where the electrical conductivity of the two components is so distinctly different it is known that in the 10–100 kHz region the phase shift (capacitive component) of the signal is close to zero and this offers inherent advantages in signal conditioning/processing (Tsochatzidis et al., 1992; Fossa, 1998; Karapantsios and Papara, 2008). Frequency scanning showed that an excitation frequency of 25 kHz provides the lowest phase shift (less than 1°) and thus almost pure resistive behavior. The input current creates a voltage drop due to the finite (but variable) resistance of the two-phase medium (R_m) and exits from another ring electrode. This electrode is connected to the one end of a termination resistor (R_t), while the other end of the resistor is grounded. R_m and R_t constitute a voltage divider and the voltage across the termination resistor is the measured output voltage V_o. V_i and V_o are recorded by a high-resolution 24 bit data acquisition card (E-MU 1616m, CREATIVE Professional) with a sampling frequency of 192 kHz. The recorded AC signals are digitally filtered applying a band pass filter centered at 25 kHz with 1 kHz bandwidth. This reduces the total noise and makes possible to accurately measure very low voltage differentials. The envelope of the filtered AC signals is then digitally extracted by taking the absolute value using a Matlab routine. This process is non-linear and therefore creates high frequency artifacts, which are removed by applying a low pass filter with cut-off frequency of 100 Hz. The so-filtered envelope of the signals V_i and V_o is the actual peak voltage amplitude of the signals without any loss of information or distortion. Since R_m and R_t constitute a voltage divider, R_m is simply calculated from the relation $V_o/V_i = R_t/(R_m + R_t)$. For the range of void fraction values studied in this work (10^{-3}–10^{-1}), Maxwell's model (Maxwell, 1892) is chosen for void fraction determination from electrical impedance data. The final output of data reduction is several records of 60 s-long void fraction time series for different experimental conditions.

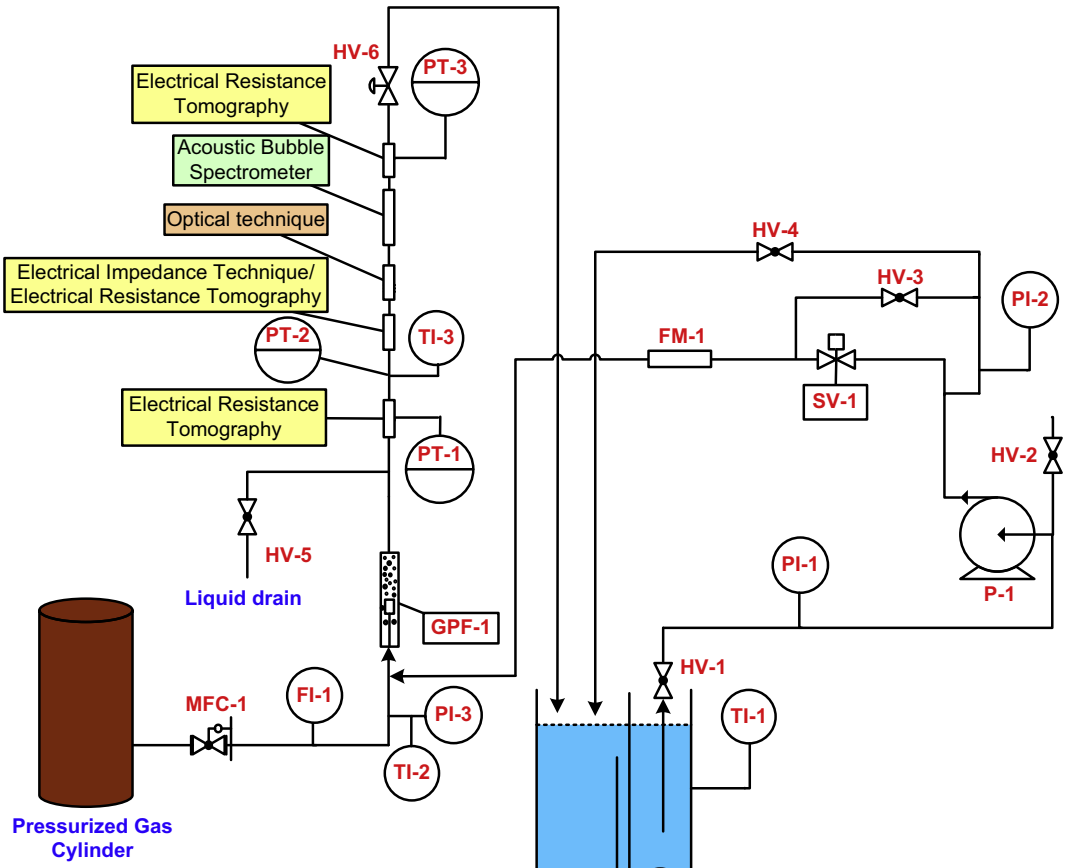

Code	Description
T-1	Liquid Tank
P-1	Progressive Cavity Pump
SV-1	Proportional Electromagnetic Valve
HC-1	Heater/Circulator
FM-1	Liquid Flow Meter
MFC-1	Gas Mass Flow Controller
FI-1	Gas Flow Meter
GPF-1	Glass Porous Filter
HV-1,2,3,4,5	On/Off Hand Valves
HV-6	Screw Down Hand Valve
TI-1,2,3	Temperature Indicators
PI-1,2,3	Pressure Indicators
PT-1,3	Differential Pressure Transducers
PT-2	Absolute Pressure Transducer

Fig. 1. Experimental setup.

Electrical impedance measurements are performed by a pair of ring electrodes which are flush-mounted to the inner walls of the test tube in order to avoid disturbing the flow. Based on previous experimental evidence (Tsochatzidis et al., 1992; Karapantsios et al., 1989; Devia and Fossa 2003) and extensive preliminary tests herein, we concluded in an electrodes' separation distance of $D/4$ and an electrode width of $D/10$ in order to assure reliable average void fraction measurements and ample signal fluctuations at the same time. The pair of ring electrodes is located at a distance of 59 cm (~28D) above the gas injection point. It is reminded that the necessary entrance length for a fully developed vertical co-current upward bubbly flow is 16D for the range of superficial velocities studied in the present work (Winterton and Munaweera, 2001).

Electrical impedance measurements are taken synchronously with optical images by a technique described in detail in Evgenidis et al. (2010). High resolution images of bubbly flow are recorded at different radial positions inside the vertical tube at a distance of 75 cm above the gas injection point. These images are processed by a custom software (Zabulis et al., 2007) that estimates automatically the bubble size distribution from a large number of images according to a template matching technique. Bubble size distributions of every run are derived from image analysis of more than 500 bubbles in order to have a good statistical significance of estimations (Deckwer, 1992). Radial deviations proved insignificant (Evgenidis et al., 2010) so bubble size distributions are averages from all radial positions.

Void fraction values determined by electrical impedance measurements are validated against differential pressure measurements conducted at two locations along the flow (PT-1 and PT-3 in Fig. 1). These are performed by piezo-electrical ultra-sensitive sensors (DP 15, Validyne Engineering) combined with a proper signal demodulator (CD280, Validyne). Moreover, bubbly flow homogeneity and symmetry across and along the vertical tube is evaluated by means of an Electrical Resistance Tomography (ERT) technique (P2000, ITS). Three similar probes consisting of 16

Table 1
Measured physical properties of the employed test liquids at 37 °C.

Test liquid	Composition	SDS (ppm)	Surface tension (mN/m)	Density (kg/m^3)	Electrical conductivity (mS/cm)*	Dynamic viscosity (mPa s)
Water	NaCl (0.02% w/w) aqueous solution	5	67.0	995	0.5	0.70
		500	37.0	991	0.5	0.70
Blood	Glycerol (56.0% w/w)/NaCl (1.3% w/w) aqueous solution	–	68.0	1149	5.4	4.85
		500	34.0	1144	5.4	5.10

* Measured at 25 °C.

flush-mounted plate electrodes (2 mm × 2 mm) made of stainless steel provide ERT measurements at three different heights (planes) in the vertical tube, with a sampling frequency of 16 Hz. The distance of ERT probes from the gas injection point is 21.5 cm, 62.0 cm and 116.5 cm. Bubble homogeneity is confirmed for all experimental conditions (Hatzidafni et al., 2009). Typical ERT images are presented in Supplementary Fig. 1. It is mentioned that differential pressure measurements are found to confirm electrical ones (performed either with the impedance technique or ERT) in terms of estimated void fraction values to within ±10% of each value without any noticed persistent trend (Evgenidis, 2011).

Experiments are performed at 37 °C, same as body temperature, in two different test liquids. The first one is an aqueous solution of NaCl (purity > 99.5%, Merck KGaA), hereafter be called *Water*, resembling the electrical conductivity of tap water. The second one is an aqueous solution of glycerol (purity > 99.5%, Panreac) and NaCl, hereafter be called *Blood*, simulating human blood physical properties (electrical conductivity ~5.4 mS/cm, dynamic viscosity 4–5 mPa s, pH ~7.5; Woodcock, 1975; Dorsey, 1940). All the measured physical properties of the test liquids at 37 °C are shown in Table 1. Helium gas (purity 99.9996%, Air Liquide) is chosen for bubbles production due to its low solubility in the test liquids.

Measurements are conducted for two bubble populations having different average bubble sizes, both below 1 mm. Preliminary tests show that the addition of 5 ppm and 500 ppm of the surface active agent sodium dodecyl sulphate (SDS, purity > 99.0%, Fluka Biochemika) in *Water* provided fairly distinct bubble size distributions. This is also the case for *Blood* when no SDS is added and with the addition of 500 ppm SDS. All resulting bubble size distributions are well-fitted by log-normal curves as rather expected for this type of application (e.g. Camarasa et al., 1999; Evgenidis et al., 2010). An indicative log-normal fitted bubble size distribution is given in Supplementary Fig. 2.

Five different liquid superficial velocities (2.89, 9.62, 16.36, 23.10, 29.83 cm/s) as well as eight different gas superficial velocities (0.048, 0.132, 0.217, 0.301, 0.385, 0.650, 0.914, 1.179 cm/s) are examined. Liquid superficial velocity values range from ~3 to ~30 cm/s, as these values are representative of bloodstream in human vena cava. On the other hand, gas superficial velocity values range from 0.05 to 1.2 cm/s providing average void fraction values between $\sim10^{-3}$ and $\sim10^{-1}$. In all cases, the combination of superficial liquid and gas velocities results in bubbly flow pattern, in accordance to Taitel et al. (1980). It is noted that average void fraction values above 0.05 are high and not representative of mild DCS incidents in humans, yet they are important for the completeness of this study.

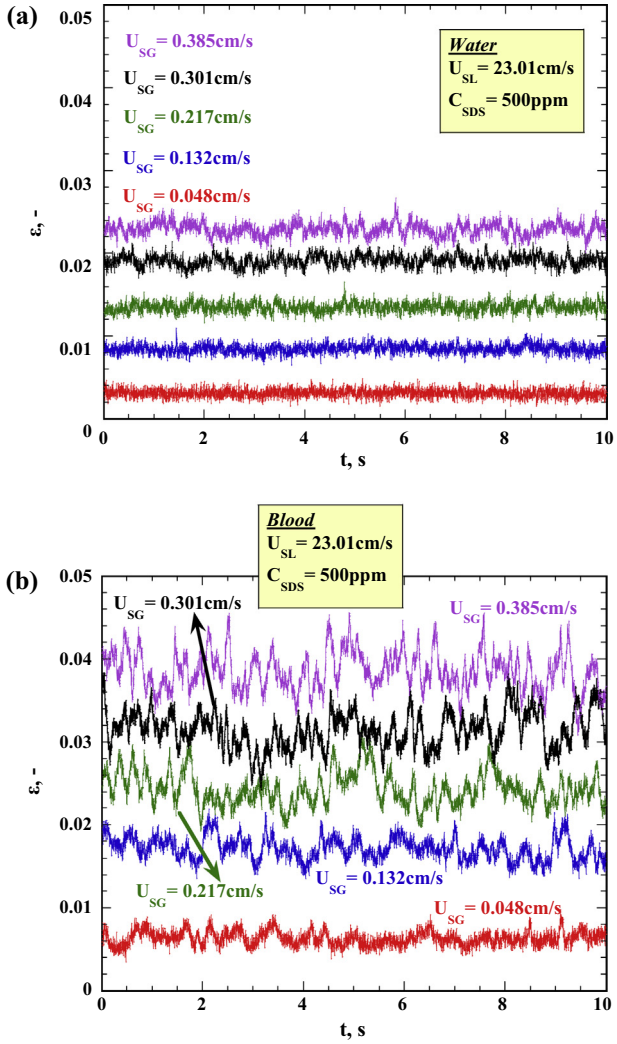

Fig. 2. Effect of gas superficial velocity (U_{SG}) on void fraction time series for (a) *Water* (U_{SL} = 23.01 cm/s, C_{SDS} = 500 ppm) and (b) *Blood* (U_{SL} = 23.01 cm/s, C_{SDS} = 500 ppm).

Results and discussion

i. Void fraction signals

Figs. 2–4 present void fraction, ε, versus time for only 10 s in order to discern some signal features. In all cases, void fraction fluctuates around an average value with frequency and intensity that differ among experimental conditions. Since electrical signals are smooth in the absence of gas bubbles (fluctuations are an order of magnitude lower than at any bubbly flow conditions), it is apparent that fluctuations are caused by the flow of bubbles. A few spikes noticed in some signals correspond to individual larger bubbles. The impedance technique can sense these bubbles over and above smaller bubbles. From basic principles (Tsochatzidis et al., 1992) it is expected that void fraction fluctuations increase in intensity when a bubble size distribution gets wider with large bubbles flowing together with small bubbles. On the contrary, the frequency of void fraction fluctuations does not show a clear dependence in frequency when the number of bubbles increases.

Fig. 2 shows the effect of gas superficial velocity, U_{SG} on void fraction signals for a constant value of liquid superficial velocity, U_{SL}, and surfactant concentration C_{SDS}, in *Water* and *Blood*. As U_{SG} increases not only the mean level of the signal but also the intensity of fluctuations increases. This is because the gas volume increases which also means more and in some cases also larger bubbles (see below) appear in the flow. This trend is consistent with other works, such as Godbole et al. (2011) and Bhagwat and Ghajar (2012). The increase is different in *Blood* than in *Water*. This indicates that although the increase of gas volume with U_{SG} is alike in the two liquids, the number and size of bubbles are different as result of the different physicochemical properties of the two liquids.

Fig. 3 shows that the mean level of the void fraction signal decreases in both liquids when U_{SL} increases for a constant value of U_{SG} and C_{SDS}. As U_{SL} increases, bubbles flow with higher velocity and consequently their residence time inside the measuring volume decreases leading to lower void fractions. The same observation has been also made by Godbole et al. (2011) and Zhao et al. (2013). What is of greater significance to this work is the effect of U_{SL} to signal fluctuations. As U_{SL} increases, fluctuations become less intense in both liquids. This is again different in *Blood* than in *Water*. Although differences are not as prominent as in Fig. 2, they might be once more attributed to the different features of bubble size distributions.

Influence of SDS concentration on void fraction signals is illustrated in Fig. 4. Addition of SDS lowers the liquid surface tension and also increases the elasticity of bubble films which hinders their coalescence to larger bubbles (e.g. Xu et al., 2009). Thus, a larger amount of smaller bubbles rise inside the tube. As bubbles get smaller, their buoyant velocity decreases and accordingly their residence time in the tube increases yielding higher void fractions. Using liquid viscosity values from Table 1 and Stokes law (valid for mobile-surfactant free- surfaces) it is found that buoyant velocity is less than 10% of U_{SL} when bubbles are smaller than 100 micrometers in *Water* and smaller than 300 micrometers in *Blood*. So, based on bubble size alone, one would not expect such large difference between signals in Fig. 4b. The observed difference is because of the immobility of bubble surfaces brought about by the presence of the adsorbed surfactant layer in terms of film elasticity and Marangoni stresses. Both effects increase drag coefficient towards that of a rigid sphere and retards surface motion. Thus, bubbles rise with lower velocity and so void fraction increases (Alves et al., 2005). Concerning signal fluctuations' dependence on SDS concentration, the two test liquids show opposing trends. Increase of surface-active concentration lowers a bit the intensity of signal undulations for the case of *Water* but on the contrary intensifies considerably the fluctuations for *Blood*. Again, this manifests different bubble size distributions in the two liquids.

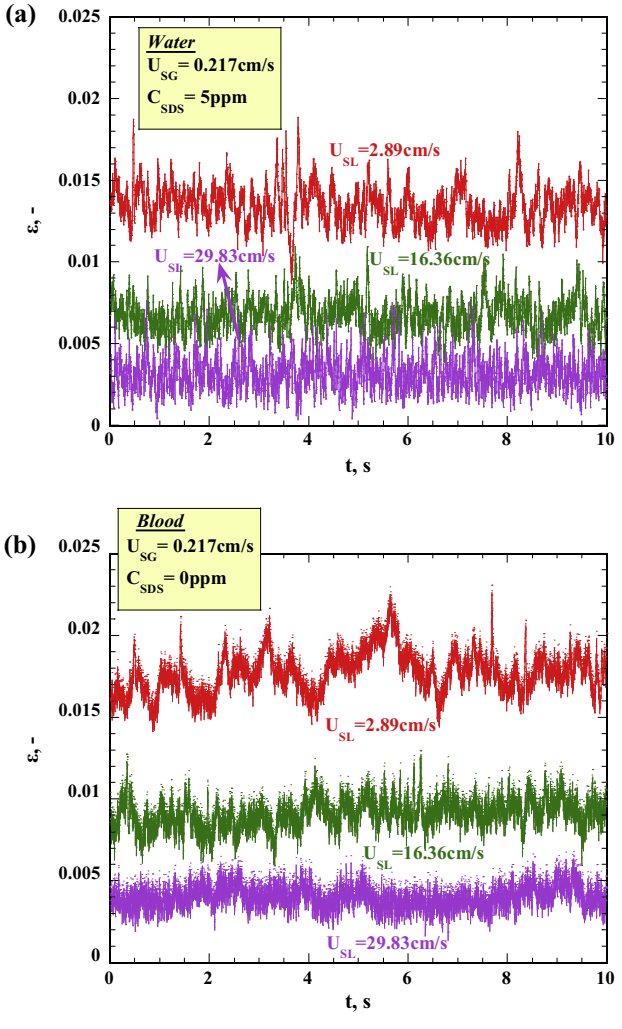

Fig. 3. Effect of liquid superficial velocity (U_{SL}) on void fraction time series for (a) *Water* (U_{SG} = 0.217 cm/s, C_{SDS} = 5 ppm) and (b) *Blood* (U_{SG} = 0.217 cm/s, C_{SDS} = 0 ppm).

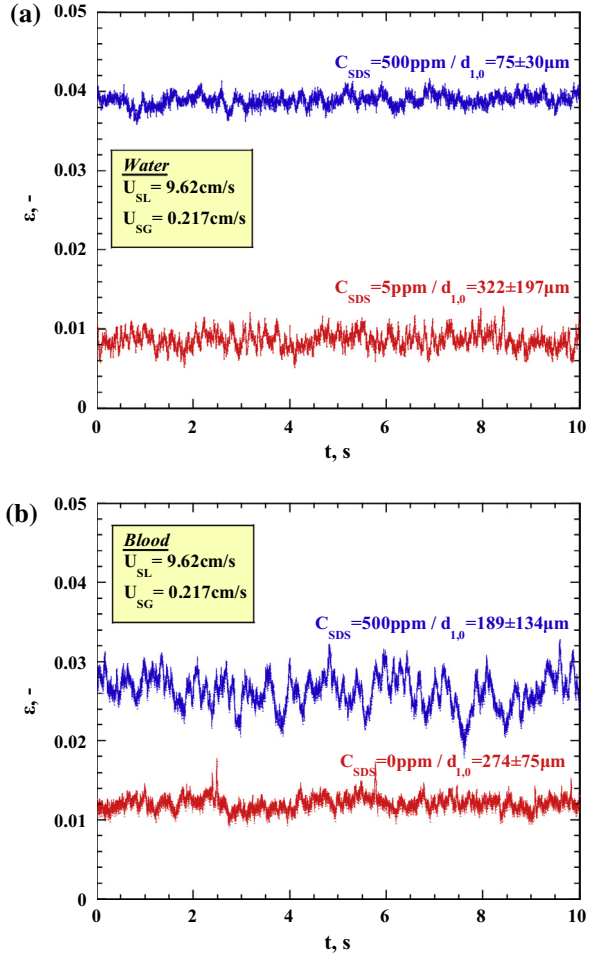

Fig. 4. Effect of SDS concentration (C_{SDS}) on void fraction time series for (a) *Water* (U_{SL} = 9.62 cm/s, U_{SG} = 0.217 cm/s) and (b) *Blood* (U_{SL} = 9.62 cm/s, U_{SG} = 0.217 cm/s).

ii. Statistics of void fraction and bubble size

Detailed examination of flow conditions and physicochemical properties of the two test liquids on bubble size distributions is away from the objectives of this work and can be found in Evgenidis et al. (2010) and Evgenidis (2011). Here it is adequate to show that the average bubble size and the standard deviation of bubble size are associated with clear trends in void fraction signals. However, the physical mechanisms that control the bubble size are briefly discussed with regards Fig. 5 which presents the effect of surfactant and electrolyte addition as well as of liquid viscosity on typical bubble size distributions. Increase of SDS concentration makes bubbles smaller due to surface tension decrease and coalescence hindrance in both liquids (*Water*- Fig. 5a, *Blood*- Fig. 5b). Comparing bubble size distribution for C_{SDS} = 5 ppm in *Water* (Fig. 5a) with the one for C_{SDS} = 0 ppm in *Blood* (Fig. 5b), it is shown that bubble size is reduced in *Blood* despite the lack of surface active agent. This is attributed to the much higher concentration of electrolyte (NaCl) that further promotes the coalescence hindrance by means of electrical repulsive forces (Xu et al., 2009). On the contrary, the moderate increase of liquid viscosity in *Blood* as compared to *Water* does not seem to affect bubble size, since the dissipation forces are not strong enough to promote coalescence in this range of viscosity values (Ruzicka et al., 2003).

The addition of 500 ppm SDS to either *Water* or *Blood* will be henceforth referred to as the *Small* bubbles case, while the absence of SDS in *Blood* or the addition of 5 ppm SDS to *Water* will be henceforth referred to as the *Large* bubbles case.

Average and standard deviation

Figs. 6–9 display the influence of the SDS concentration (C_{SDS}), superficial liquid velocity (U_{SL}) and superficial gas velocity (U_{SG}) on the average value and the standard deviation of void fraction -ε_{ave}, StDev(ε)- and bubble diameter -$d_{1,0}$, StDev($d_{1,0}$)- respectively. Standard deviation is an integral way to quantify the intensity of

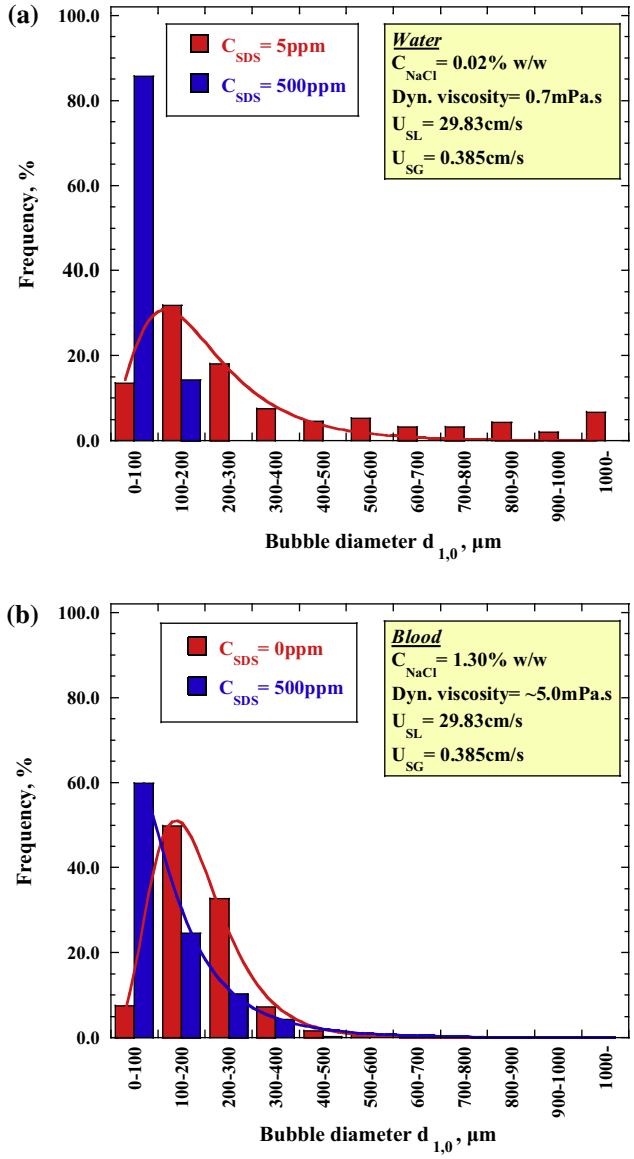

Fig. 5. Effect of SDS, NaCl concentration and liquid viscosity on bubble size distributions: (a) *Water* (U_{SL} = 29.83 cm/s, U_{SG} = 0.385 cm/s) and (b) *Blood* (U_{SL} = 29.83 cm/s, U_{SG} = 0.385 cm/s).

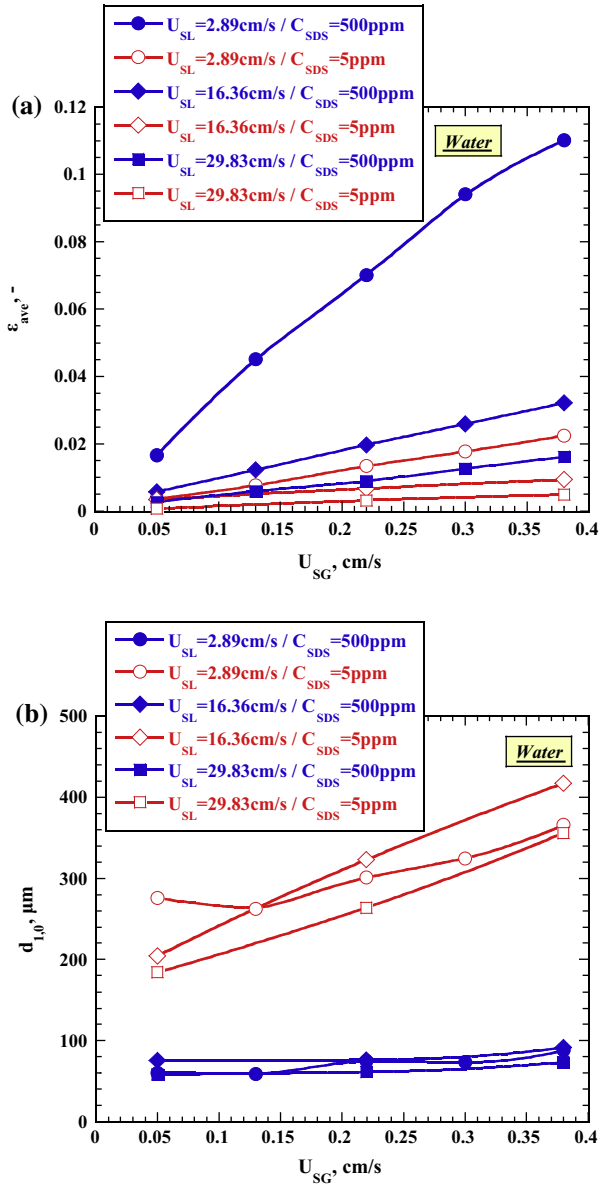

Fig. 6. Effect of SDS concentration (C_{SDS}), superficial liquid velocity (U_{SL}) and superficial gas velocity (U_{SG}) on the average values of (a) void fraction, ε_{ave} and (b) bubble diameter, $d_{1,0}$, for *Water*.

fluctuations around the average value of the entire void fraction time series. In the plots, red curves correspond to the *Large* bubbles case while blue curves correspond to the *Small* bubbles case.

Figs. 6 and 7 present results for *Water*. As discussed in the previous section, average void fraction, ε_{ave}, increases with rising U_{SG} (more bubbles) and C_{SDS} (smaller bubbles) but decreases with rising U_{SL} (lower residence time of bubbles), Fig. 6a. On the other hand, the average bubble size $d_{1,0}$, is essentially unaffected by U_{SG} and U_{SL} with the *Small* bubbles (less than 100 μm) but with the *Large* bubbles (between 200 and 400 μm) $d_{1,0}$ increases with U_{SG} and decreases with U_{SL} (U_{SL} = 2.89 cm/s value is repeatable, yet strange). Moreover, $d_{1,0}$ clearly decreases with C_{SDS}, Fig. 6b. It must be noted that results on $d_{1,0}$ reflect phenomena happening during gas injection (shearing-off bubbles) and not during the upward bubbly flow in the tube. The latter may be responsible for the differences between the observed trends of ε_{ave} and $d_{1,0}$.

The standard deviation of void fraction, StDev(ε), increases with U_{SG} but decreases with C_{SDS} and U_{SL}, Fig. 7a. Furthermore, the standard deviation of bubble size, StDev($d_{1,0}$), is unaffected by U_{SG} and U_{SL} with the *Small* bubbles but with the *Large* bubbles it increases with both U_{SG} and U_{SL}, Fig. 7b. To this end, in *Water* the average size $d_{1,0}$ of *Large* bubbles are associated with smaller ε_{ave} and larger StDev(ε) whereas $d_{1,0}$ of *Small* bubbles are associated with larger ε_{ave} and smaller StDev(ε). In other words, in *Water* average bubble size is inversely proportional to average void fraction and directly proportional to void fraction fluctuations.

Figs. 8 and 9 present the same parameters as Figs. 6 and 7 but for *Blood*. As regards the variation of average void fraction, ε_{ave}, and average bubble size, $d_{1,0}$, with U_{SG}, C_{SDS} and U_{SL}, qualitatively similar arguments hold as in *Water*. Only that now in Blood, *Small* bubbles (C_{SDS} = 500 ppm) are a bit larger (~100–150 μm) than in *Water* (<100 μm) at similar conditions. This is rather the reason for the alike average void fraction values with *Water*, Fig. 8. Even more interesting is that in *Blood* the standard deviation of the average void fraction, StDev(ε), and that of the average bubble size, StDev ($d_{1,0}$), for the *Small* and the *Large* bubbles behave exactly the opposite than in *Water*, Fig. 9. That is, for the *Small* bubbles (blue lines) there is a clearly higher standard deviation than for the *Large* bubbles (red lines) at the same gas and liquid flow rates. At first glance this is counter intuitive as one would expect larger bubbles to present more intense size fluctuations and also yield lower average void fractions.

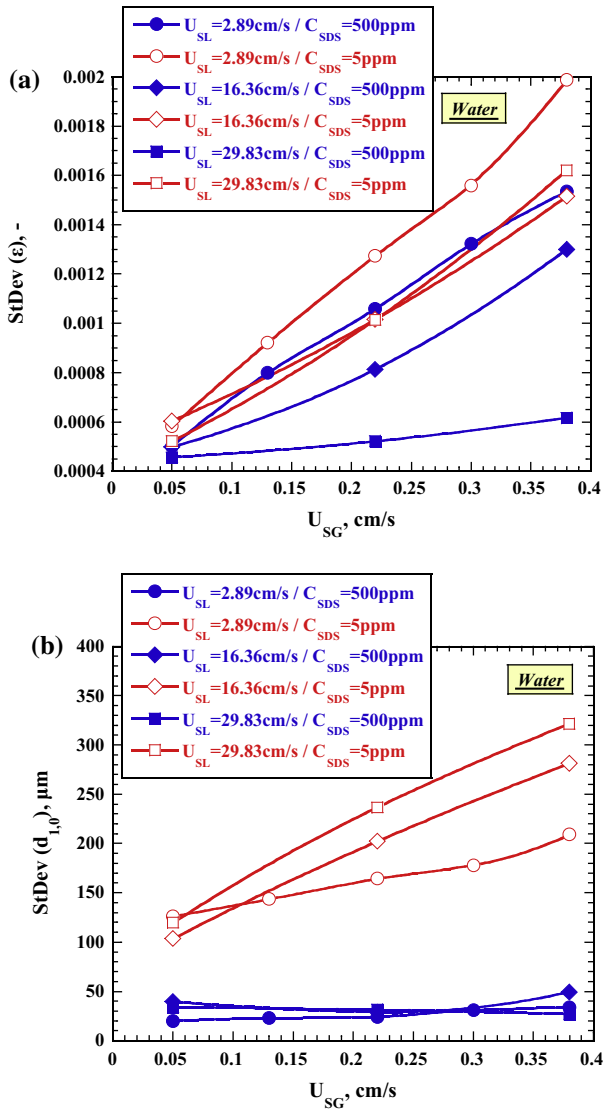

Fig. 7. Effect of SDS concentration (C_{SDS}), superficial liquid velocity (U_{SL}) and superficial gas velocity (U_{SG}) on the standard deviation values of (a) void fraction StDev(ε) and (b) bubble diameter StDev($d_{1,0}$), for *Water*.

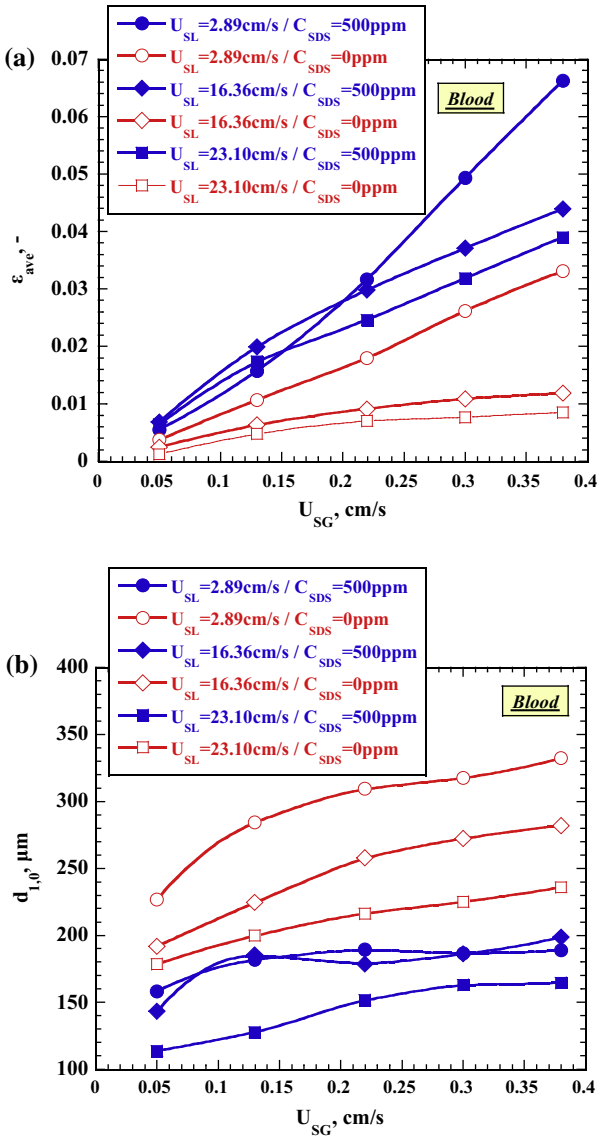

Fig. 8. Effect of SDS concentration (C_{SDS}), superficial liquid velocity (U_{SL}) and superficial gas velocity (U_{SG}) on the average values of (a) void fraction ε_{ave} and (b) bubble diameter $d_{1,0}$, for *Blood*.

The answer lies at the geometrical characteristics of *Small* bubbles as they appear in *Blood*. For the examined liquid and gas flow rates, the size distribution of bubbles seems to depend strongly on both surfactant and electrolyte concentration (Evgenidis et al., 2010). When surfactant and electrolyte coexist, bubble coalescence is hindered to a greater extent than if they were alone in the liquid phase. Yet, the presence of surfactant along with the finite salinity, surface tension and viscosity of *Blood* allows the formation of stable bubble clusters (Fig. 10) –a floc-like structure consisting of many bubbles- that rise inside the tube among numerous other isolated bubbles. The equivalent diameter of bubble clusters range from 500 to 700 μm, whereas $d_{1,0}$ ranges from 100 to 150 μm. The number of these clusters is not large enough to change considerably $d_{1,0}$, but it is still adequate to increase StDev($d_{1,0}$). Such clusters are not seen in the *Large* bubble cases (when no surfactant is present). In-depth study of cluster behavior is beyond the scope of the present paper, but in any case their presence explains the peculiar statistics of void fraction and bubbles size for the *Small* bubble cases in *Blood*. To this end, in *Blood* the average size $d_{1,0}$ of *Large* bubbles are associated with smaller ε_{ave} and smaller StDev(ε) whereas $d_{1,0}$ of *Small* bubbles are associated with larger ε_{ave} and larger StDev(ε). In other words, in *Blood* average bubble size is inversely proportional to both average void fraction and void fraction fluctuations.

Wrapping up, an increase of surfactant concentration:

(i) Decreases $d_{1,0}$ inducing an increase of ε_{ave} in both liquids.
(ii) Affects in a different way the StDev($d_{1,0}$) and StDev(ε) of each liquid. Specifically, in *Water* it decreases StDev($d_{1,0}$) and StDev(ε) whereas in *Blood* it increases StDev($d_{1,0}$) and StDev(ε) because of bubble clusters formation.

All in all, the average void fraction is negatively correlated with average bubble size whereas the standard deviation of void fraction is positively correlated with the standard deviation of bubble size.

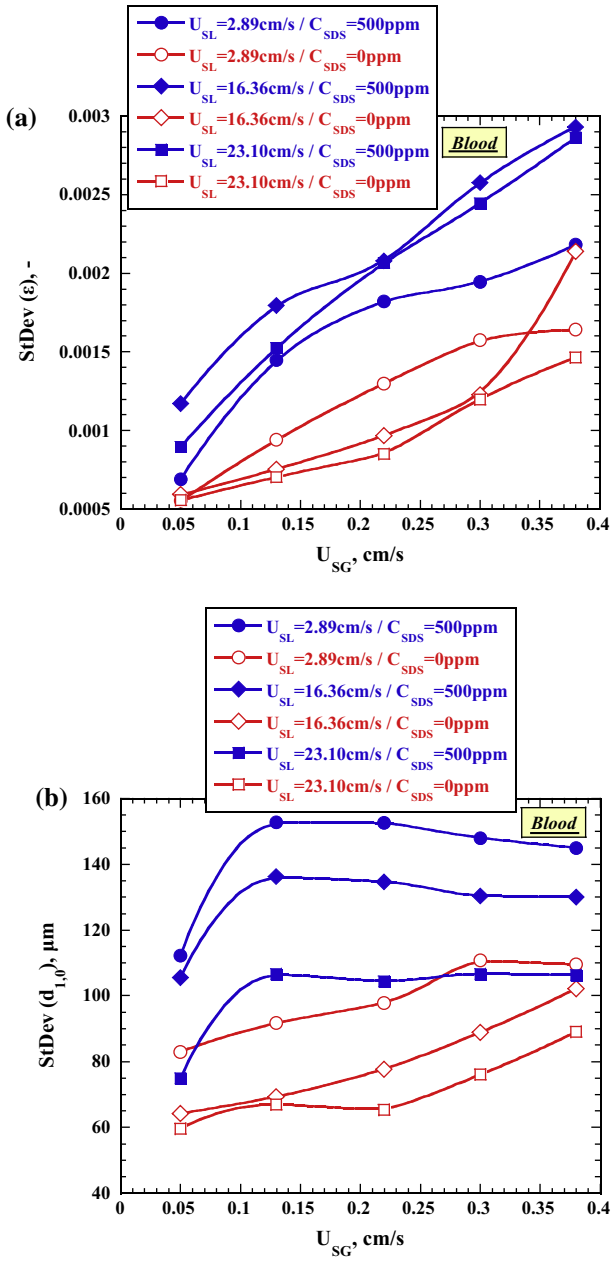

Fig. 9. Effect of SDS concentration (C_{SDS}), superficial liquid velocity (U_{SL}) and superficial gas velocity (U_{SG}) on the standard deviation values of (a) void fraction StDev(ε) and (b) bubble diameter StDev($d_{1,0}$), for *Blood*.

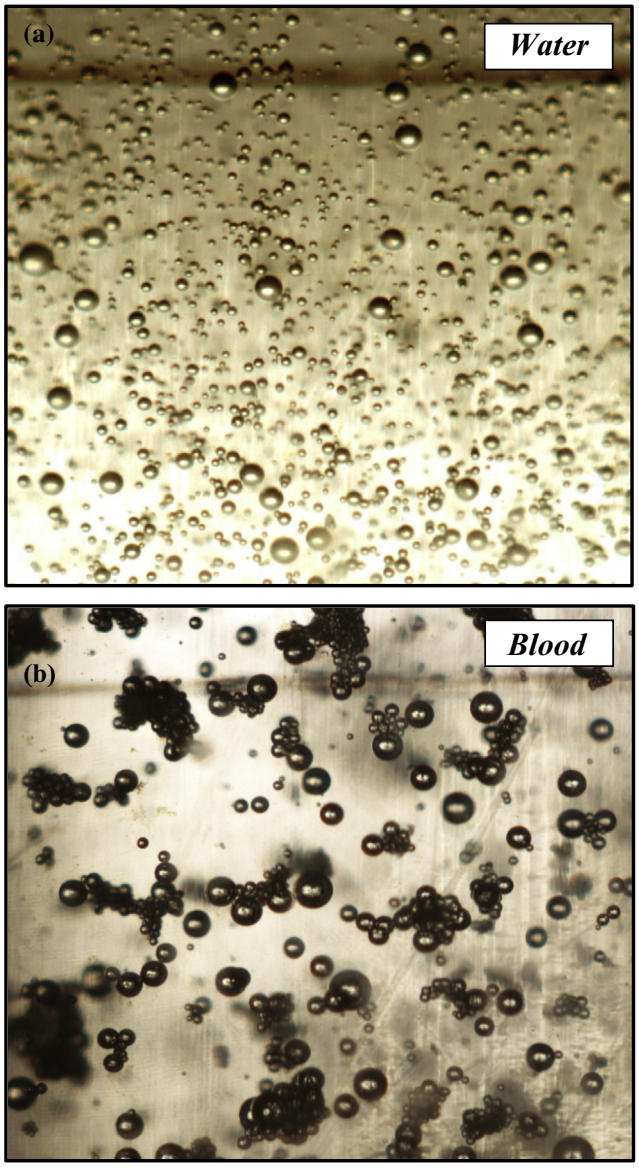

Fig. 10. Comparison of (a) isolated bubbles (in *Water*) with (b) bubble clusters (in *Blood*), C_{SDS} = 500 ppm, U_{SL} = 9.62 cm/s, U_{SG} = 0.048 cm/s.

Higher order statistics

Modal and median values calculated for void fraction time series and bubble size distributions provide similar trends with the average values. Apart from them, higher-order moments are applied for investigating the degree of symmetry of void fraction time series. Skewness and kurtosis values for all void fraction time series are pretty close to zero without any persistent trend. This indicates that void fraction data are distributed around their average value in a fairly Gaussian manner (normal distribution). One might think that the apparent symmetry of void fraction data contradicts the observed log-normal bubble size distribution (skewed to the right, i.e., to larger sizes) as reported by Evgenidis et al. (2010). However, this is not the case since void fraction signals imprint a dynamic state of a flowing bubble size distribution where larger bubbles contribute less to void fraction due to their higher rising velocity and this explains why electrical signals seem so symmetric.

Void fraction time series are further investigated by autocorrelation and spectral analysis, in an effort to reveal any masked periodicities. Autocorrelation analysis –plots not shown due to space limitations- illustrates the strong stochastic character of void fraction time series. Autocolleration function decays to zero in less than 0.1 s time interval without any clear dependence on experimental conditions. Fig. 11 presents the influence of SDS concentration on the spectral analysis of void fraction time series by employing FFT analysis to both test liquids. Spectra intensity (Y axis in Fig. 11) is much higher in *Blood* than in *Water* for similar experimental conditions, probably because of the presence of bubble clusters. Apart from that, all spectra lines follow the same pattern, i.e., decay fast with frequency. For the case of *Water* (Fig. 11a), a larger SDS concentration -500 ppm; smaller $d_{1,0}$ and StDev($d_{1,0}$)- is associated with lower spectra intensity and narrower frequency range. On the other hand, for *Blood* (Fig. 11b), SDS addition -500 ppm; smaller $d_{1,0}$ but larger StDev($d_{1,0}$)- is associated with more intense spectra of broader frequency range most probably because of the presence of clusters. In other words, the intensity and frequency range of the FFT spectra are related more with the fluctuations of bubble size, StDev($d_{1,0}$), rather than the average bubble size, $d_{1,0}$. This observation agrees with the main output above that void fraction fluctuations are associated with bubble size fluctuations. Intuitively, the frequency of void fraction fluctuations may also depend on fluctuations of bubble density (number) which is a complex function of bubble size distribution and flow rate and requires more work to quantify.

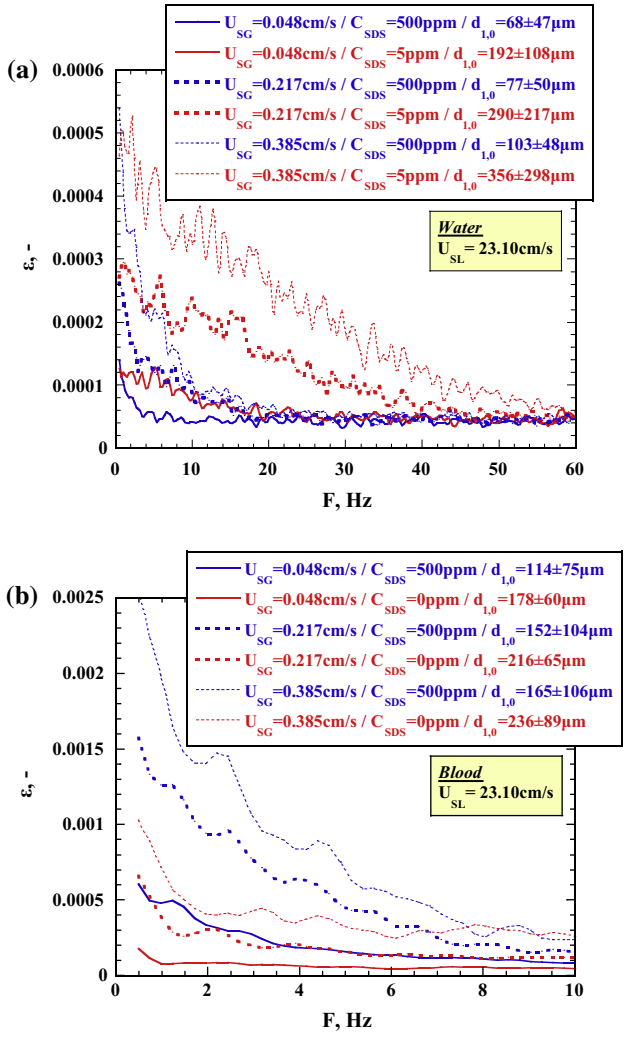

Fig. 11. Effect of SDS concentration (C_{SDS}), superficial liquid velocity (U_{SL}) and superficial gas velocity (U_{SG}) on the FFT spectrum of void fraction time series for (a) *Water* (U_{SL} = 23.10 cm/s) and (b) *Blood* (U_{SL} = 23.10 cm/s).

Correlation between statistical properties of void fraction and bubble size

In an effort to elucidate the relationship between statistical quantities of void fraction and bubble size a functional dependence is inquired. Information from dimensional analysis as well as other efforts in literature suggest an empirical expression of the form:

$$\text{Bubble size statistical quantity} = f(\text{void fraction statistical quantity}, U_{SG}/U_{SL}) \quad (1)$$

which after extensive trials (Evgenidis, 2011) takes the form:

$$\text{Bubble size statistical quantity} = a(\text{void fraction statistical quantity})^{b}(U_{SG}/U_{SL})^{c} \quad (2)$$

All terms above are dimensionless. The presence of the term U_{SG}/U_{SL} proved necessary, although it is partially correlated to average void fraction, as this allows separating the statistical weight of void fraction fluctuations from that of average void fraction. Table 2 summarizes the results of fitting the above formula to the data of this study (analysis by Matlab Signal Processing toolkit) within the range of the examined parameters.

Table 2
Results of fitting Eq. (2) to the data of the present study (Y: bubble size statistical quantity, $X1$: void fraction statistical quantity, $X2$: U_{SG}/U_{SL}, D: tube diameter) – W: *Water*, B: *Blood*.

#	Liquid	Y	$X1$	$X2$	R^2	Mean absolute percentage error (MAPE), %
1	W	$d_{1,0}/D$	StDev(ε)	U_{SG}/U_{SL}	0.7	43.9
2	B	$d_{1,0}/D$	StDev(ε)	U_{SG}/U_{SL}	0.53	20.3
3	W + B	$d_{1,0}/D$	StDev(ε)	U_{SG}/U_{SL}	0.54	59.2
4	W	StDev($d_{1,0}$)/D	StDev(ε)	U_{SG}/U_{SL}	0.67	54.8
5	B	StDev($d_{1,0}$)/D	StDev(ε)	U_{SG}/U_{SL}	0.54	14.8
6	W + B	StDev($d_{1,0}$)/D	StDev(ε)	U_{SG}/U_{SL}	0.54	59.9
7	W	StDev($d_{1,0}$)/$d_{1,0}$	StDev(ε)/ε_{ave}	U_{SG}/U_{SL}	0.59	13.8
8	B	StDev($d_{1,0}$)/$d_{1,0}$	StDev(ε)/ε_{ave}	U_{SG}/U_{SL}	0.28	28.5
9	W + B	StDev($d_{1,0}$)/$d_{1,0}$	StDev(ε)/ε_{ave}	U_{SG}/U_{SL}	0.11	29.5
10	W	StDev($d_{1,0}$)/D	ε_{ave}	U_{SG}/U_{SL}	0.74	53.4
11	B	StDev($d_{1,0}$)/D	ε_{ave}	U_{SG}/U_{SL}	0.52	14.7
12	W + B	StDev($d_{1,0}$)/D	ε_{ave}	U_{SG}/U_{SL}	0.33	64.5
13	W	$d_{1,0}/D$	StDev(ε)/ε_{ave}	U_{SG}/U_{SL}	0.93	20.6
14	B	$d_{1,0}/D$	StDev(ε)/ε_{ave}	U_{SG}/U_{SL}	0.88	21.9
15	W + B	$d_{1,0}/D$	StDev(ε)/ε_{ave}	U_{SG}/U_{SL}	0.86	24.6

Shaded rows concern data for Water and Blood together.

In Table 2, expressions 13–15 offer by far a better fitting of the data taking into account both R^2 and MAPE (Mean Absolute percentage Error) values. Moreover, expression 15 provides adequate statistical significance for both examined liquids (R^2 = 0.86, MAPE = 24.6). The full form of expression 15 is:

$$\frac{d_{1,0}}{D} = 0.491\left(\frac{\mathrm{StDev}(\varepsilon)}{\varepsilon_{\mathrm{average}}}\right)^{0.827}\left(\frac{U_{SG}}{U_{SL}}\right)^{0.505} \quad (3)$$

Fig. 12a compares experimental $d_{1,0}$ values to those calculated from Eq. (3). It is seen that predictions have reasonable accuracy (±20%). This is more so if one considers that it describes so different liquids, *Water* and *Blood*, and despite the presence of bubble clusters in *Blood*. Contrary to Figs. 2–9 and 11 that showed only indicative data, Fig. 12 presents results for the whole range of the examined experimental conditions.

FFT spectra is shown (Fig. 11) to be associated with void fraction fluctuations and, additionally, show a clear dependence on experimental conditions. So an effort is made to incorporate FFT information to expression 15 of Table 2. Data analysis resulted in adding an extra term of the form $(\mathrm{FFT}_{\mathrm{area}})^d$:

$$\frac{d_{1,0}}{D} = 1.535 FFT_{area}^{0.183}\left(\frac{\mathrm{StDev}(\varepsilon)}{\varepsilon_{\mathrm{average}}}\right)^{0.802}\left(\frac{U_{SG}}{U_{SL}}\right)^{0.389} \quad (4)$$

where the term $\mathrm{FFT}_{\mathrm{area}}$ represents the area (integral) below the FFT curve normalized by the length of the frequency domain.

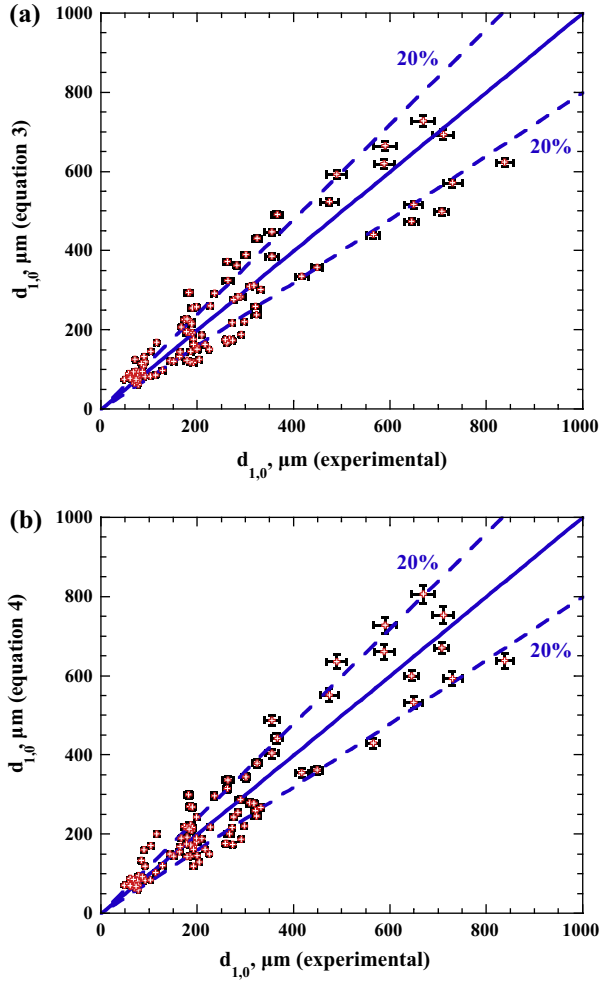

Fig. 12. Comparison of experimental and calculated $d_{1,0}$ values from (a) Eq. (3) and (b) Eq. (4).

Fig. 12b compares the experimental values of $d_{1,0}$ with those calculated from Eq. (4). Although the goodness of fitting (R^2 = 0.88) is slightly better than with Eq. (3) in Fig. 12a, Eq. (3) requires considerably less computational effort and so it may be preferred.

The above constitute only a first effort to correlate average bubble size to void fraction fluctuations. It goes without saying that more work over broader experimental conditions is required before conclusive statements can be made.

Conclusions

In the present study, fluctuations of void fraction are measured with exceptional temporal and intensity resolution by means of a novel non-intrusive electrical impedance technique in co-current upward dispersed bubble flows. Experiments are performed in water and blood-simulant that yield diverse bubble features as result of their different physicochemical properties. Bubbles size is varied using prescribed concentrations of a surfactant (SDS) while bubbles sizes are computed from optical images. Stochastic features and persistent trends of void fraction time series are discussed first qualitatively as regards their variation with gas and liquid flow rates as well as with bubble size. Then statistical analysis of void fraction time series and bubble sizes is employed to get information that allows correlation between the two quantities. It is demonstrated that the average void fraction increases when either the gas superficial velocity increases or the liquid superficial velocity and the average bubble size decreases. Of greater significance to this study is that in both liquids the intensity of void fraction fluctuations is positively correlated with the intensity of bubble size fluctuations. This is interesting if one notes the distinctly different bubble size statistics in the two liquids because of the presence of bubble clusters in blood simulant. In addition, the intensity and frequency range of the FFT spectra depends more on the intensity of bubble size fluctuations rather than the average bubble size. Elaborating more on the obtained statistical quantities, an empirical expression is derived capable of describing (±20%) the average bubble size in both liquids with respect to two experimental ratios. One is the ratio of the standard deviation over the average of void fraction and the other is the ratio of the gas over the liquid superficial velocity.

Acknowledgements

This study was funded by esa (GSTP Project: In-Vivo Embolic Detector, I-VED – Contract No.: 4000101764 and MAP Project: Convective boiling and condensation local analysis and modelling of dynamics and transfers, MANBO – Contract No.: 4200020289) and carried out under the umbrella of COST Action MP1106: 'Smart and green interfaces-from single bubbles and drops to industrial, environmental and biomedical applications'. The view expressed herein can in no way be taken to reflect the official opinion of the European Space Agency.

Appendix A. Supplementary material

Supplementary data associated with this article can be found, in the online version, at http://dx.doi.org/10.1016/j.ijmultiphaseflow.2015.05.013.

References

Alves, S.S., Orvalho, S.P., Vasconcelos, J.M.T., 2005. Effect of bubble contamination on rise velocity and mass transfer. Chem. Eng. Sci. 60, 1–9.

Andreussi, P., Di Donfrancesco, A., Messia, M., 1988. An impedance method for the measurement of liquid hold up in two-phase flow. Int. J. Multiph. Flow 14, 777–785.

Asali, J.C., Hanratty, T.J., Andreussi, P., 1985. Interfacial drag and film height in vertical annular flow. A.I.Ch.E. J. 31, 895–902.

Begovich, J.M., Watson, J.S., 1978. An electroconductivity technique for the measurement of axial variation of holdups in three-phase fluidized beds. A.I.Ch.E. J. 24, 351–354.

Bhagwat, S.M., Ghajar, A.J., 2012. Similarities and differences in the flow patterns and void fraction in vertical upward and downward two phase flow. Exp. Therm. Fluid Sci. 39, 213–227.

Camarasa, E., Vial, C., Poncin, S., Wild, G., Midoux, N., Bouillard, J., 1999. Influence of coalescence behaviour of the liquid and of gas sparging on hydrodynamics and bubble characteristics in a bubble column. Chem. Eng. Process. 38, 329–344.

Carbonell, R.G., Whitaker, S., 1984. Heat and mass transfer in porous media (121–198). In: Bear, J., Corapcioglu, M.Y. (Eds.), Fundamentals of Transport Phenomena in Porous Media. Martinus Nijhoff Publishers, Dordrecht, The Netherlands.

Ceccio, S.L., George, D.L., 1996. A review of electrical impedance techniques for the measurement of multiphase flows. J. Fluids Eng. 118, 391–399.

Celmins, A., 1988. Representation of two-phase flows by volume averaging. Int. J. Multiph. Flow 14, 81–90.

Chen, Z., Zheng, C., Feng, Y., Hoffmann, H., 1998. Local bubble behavior in three-phase fluidized beds. Can. J. Chem. Eng. 76, 315–318.

Das, A.K., Das, P.K., 2010. Modelling bubbly flow and its transitions in vertical annuli using population balance technique. Int. J. Heat Fluid Flow 31, 101–114.

Deckwer, W.D., 1992. Bubble Column Reactors. John Wiley and Sons, England.

Devia, M., Fossa, M., 2003. Design and optimisation of impedance probes for void fraction measurements. Flow Meas. Instrum. 14, 139–149.

Dorsey, N.E., 1940. Properties of ordinary water-substances, New York.

Evgenidis, S.P., 2011. Development of an electrical technique for detection and characterization of bubbles in liquid flows, PhD Thesis, Aristotle University of Thessaloniki, Greece.

Evgenidis, S.P., Kazakis, N.A., Karapantsios, T.D., 2010. Bubbly flow characteristics during decompression sickness: effect of surfactant and electrolyte on bubble size distribution. Colloids Surf. A: Physicochem. Eng. Aspects 365, 46–51.

Fossa, M., 1998. Design and performance of a conductance probe for measuring the liquid fraction in two-phase gas–liquid flows. J. Flow Meas. Instrum. 9, 103–109.

Godbole, P.V., Tang, C.C., Ghajar, A.J., 2011. Comparison of void fraction correlations for different flow patterns in upward vertical two phase flow. Heat Transf. Eng. 32 (10), 843–860.

Hatzidafni, A., Evgenidis, S., Lioumbas, I., Karapantsios, T., 2009. Electrical Resistance Tomography in upward co-current bubbly flow. In: 4th Int. Workshop "Bubble and Drop Interfaces", Thessaloniki, Greece.

Karapantsios, T.D., Evgenidis, S.P., Zacharias, K., Mesimeris, T., 2014. Method for the detection and characterization of bubbles in liquids and device therefor, resp.system, submitted to European Patent Office, Application Number EP14188200.1.

Karapantsios, T.D., Papara, M., 2008. On the design of electrical conductance probes for foam drainage applications. Assessment of ring electrodes performance and bubble size effects on measurements. Colloids Surf. A: Physicochem. Eng. Aspects 323, 139–148.

Karapantsios, T.D., Paras, S.V., Karabelas, A.J., 1989. Statistical characteristics of free falling films at high Reynolds numbers. Int. J. Multiph. Flow 15, 1–21.

Karapantsios, T.D., Tsochatzidis, N.A., Karabelas, A.J., 1993. Liquid distribution in horizontal axially rotated packed beds. Chem. Eng. Sci. 48 (8), 1427–1436.

Liu, T.J., 1993. Bubble size and entrance length effects on void development in a vertical channel. Int. J. Multiph. Flow 19, 99–113.

Maxwell, J.C., 1892. A Treatise of Electricity and Magnetism. Oxford University Press, London.

Papadopoulou, V., Eckersley, R.J., Balestra, C., Karapantsios, T.D., Tang, M.-X., 2013. A critical review of physiological bubble formation in hyperbaric decompression. Adv. Colloid Interface Sci. 191–192, 22–30.

Ruzicka, M.C., Drahos, J., Mena, P.C., Teixeira, J.A., 2003. Effect of viscosity on homogeneous–heterogeneous regime transition in bubble columns. Chem. Eng. J. 96, 15–22.

Shen, X., Mishima, K., Nakamura, H., 2005. Two-phase phase distribution in a vertical large diameter pipe. Int. J. Heat Mass Transf. 48, 211–225.

Taitel, Z., Bornea, D., Dukler, A.E., 1980. Modeling flow pattern transitions for steady upward gas-liquid flow in vertical tubes. A.I.Ch.E. J. 26, 345–354.

Tang, W.T., Fan, L.S., 1989. Hydrodynamics of a three-phase fluidized bed containing low-density particles. A.I.Ch.E. J. 35, 355–364.

Tsochatzidis, N.A., Karapantios, T.D., Kostoglou, M.V., Karabelas, A.J., 1992. A conductance method for measuring liquid fraction in pipes and packed beds. Int. J. Multiph. Flow 5, 653–667.

Uesawa, S.I., Kaneko, A., Abe, Y., 2012. Measurement of void fraction in dispersed bubbly flow containing micro-bubbles with the constant electric current method. Flow Meas. Instrum. 24, 50–62.

Vann, R.D., Butler, F.K., Mitchell, S.J., Moon, R.E., 2011. Decompression illness. The Lancet 377, 153–164.

Winterton, R.H.S., Munaweera, J.S., 2001. Bubble size in two-phase gas–liquid bubbly flow in ducts. Chem. Eng. Process. 40, 437–447.

Woodcock, J.P., 1975. Physical properties of blood and their influence on blood-flow measurement. Rep. Prog. Phys. 39, 65–127.

Xu, Q., Nakajima, M., Ichikawa, S., Nakamura, N., Roy, P., Okadome, H., Shiina, T., 2009. Effects of surfactant and electrolyte concentrations on bubble formation and stabilization. J. Colloid Interface Sci. 332, 208–214.

Zabulis, X., Papara, M., Chatziargyriou, A., Karapantsios, T.D., 2007. Detection of densely dispersed spherical bubbles in digital images based on a template matching technique: application to wet foams. Colloids Surf. A: Physicochem. Eng. Aspects 309, 96–106.

Zhao, Y., Bi, Q., Hu, R., 2013. Recognition and measurement in the flow pattern and void fraction of gas–liquid two-phase flow in vertical upward pipes using the gamma densitometer. Appl. Therm. Eng. 60, 398–410.